Selective and Stable Non-Noble Metal Intermetallic Compound Catalyst for the Direct Dehydrogenation of Propane to Propylene

Yang He,[†] Yuanjun Song,[†] David A. Cullen,[‡] and Siris Laursen[*,†]

[†]*Department of Chemical and Biomolecular Engineering, University of Tennessee, Knoxville, Tennessee 37996, United States*

[‡]*Materials Science and Technology Division and Center for Nanophase Materials Sciences, Oak Ridge National Laboratory, Oak Ridge, Tennessee 37831, United States*

E-mail: slaursen@utk.edu

Phone: +1 865 9745786

Content

How the Catalyst was Discovered

In an effort to develop inexpensive non-noble metal catalysts, we have focused upon understanding the surface and catalytic chemistry of non-noble transition metal (TM) IMCs and ceramics as a function of constituent element, bulk stoichiometry, and surface composition. Through in-depth, systematic computational surface science studies, experimental synthesis

development, and catalyst performance tests, a suite of IMC and TM ceramic materials with special low surface reactivity towards C=C bonds and unique reactivity towards hydrogen have been isolated as promising catalytic materials for the catalytic production of aromatics and olefins.[1–4] These studies have lead us to the discovery of the Ni+Ga catalyst presented herein.

Experimental Methods

Synthesis Method

All Al_2O_3 supported Ni+Ga catalysts (10 wt%) were synthesized by a hydroxide deposition method using $Ni(NO_3)_2$*$6H_2O$ (Sigma Aldrich) and $Ga(NO_3)_3$*xH_2O (Sigma Aldrich) as metal precursors and alumina (Alfa Aesar) as support material. During the synthesis process, $Ga(NO_3)_3$*xH_2O was first dissolved into 150 ml D.I. water at 70°C. Diluted NaOH solution was used to transform the Ga precursor into a hydroxide-nitrate at the pH of 3.9. Al_2O_3 was then input into the solution and aged for 0.5 hour. Next, specific amount of $Ni(NO_3)_2$*$6H_2O$ (based on Ni:Ga actual loading) was introduced and transformed into the hydroxide-nitrate form at the pH of 7.0. The solution was then aged for another 0.5 hour. The sample was washed, filtered, and then dried under air at 100°C for 3 hours. The dried powder was reduced at 500°C by 2% H_2/Ar for 1 hour and annealed at 700°C under Ar for 12 hours.

Our synthesis investigations suggested that the bulk stoichiometry of Ni+Ga catalysts synthesized by hydroxide method can be controlled by reduction temperature. Figure S3 showed two materials synthesized via the hydroxide method described above with a actual loading of 1:1 Ni:Ga for both. The one with the reduction temperature at 500°C displayed a Ni_3Ga bulk crystal structure whereas the other one that underwent a reduction at 700°C with pure H_2 showed a NiGa bulk crystal structure.

SiO_2 supported Ni+Ga (10 wt%) and oxide supported Ga catalysts were prepared using incipient wetness impregnation method. For oxide supported Ga materials, 5.4 wt% Ga was

loaded on Al_2O_3 support to mimic the amount of Ga in Ga-rich Ni_3Ga/Al_2O_3 catalyst and 2.8 wt% of Ga was loaded on SiO_2 support to mimic the amount of Ga bulk-like Ni_3Ga/SiO_2 catalyst. Ni_3Ga/SiO_2 with small particle size was produced after a reduction by pure H_2 at 700°C for 2 hours. Large particles of Ni_3Ga/SiO_2 were obtained via an annealing treatment for 12 hours under Ar after reduction. All samples were pretreated *in-situ* in the reactor and used directly to avoid contacting with air. Before any characterization, passivation was performed under 1% O_2/Ar at room temperature for 1hr to protect the sample from further oxidation by air and the sample reduced *in situ* in the characterization apparatus. This was not possible for the TEM studies.

Incipient wetness impregnation method was utilized to synthesize Al_2O_3 supported Pt-Sn (mimic Oleflex from UOP) and CrO_x (mimic Catofin process from CB&I Lummus) catalysts to compare our Ni+Ga IMC catalyst to the commercialized catalysts. For Pt-Sn catalyst, 1.5 wt% Pt, 1.2 wt% Sn, and 0.8 wt% K were utilized. For CrO_x, 20 wt% and 1.2 wt% K were applied. The specifically compositions chosen for Pt-Sn and CrO_x catalysts were closed to those utilized in industry.[5–7] The Pt-Sn and CrOx catalysts were then dried under air overnight at 100°C. Pt-Sn was then followed a calcination pretreatment at 560°C for 3 hours and an in-situ reduction process for 1 hour at 590°C before propane dehydrogenation reaction. For CrO_x catalyst, it was calcined for 6 hours at 600°C before the reaction.

Catalytic Activity Test

Catalytic activity tests were performed at a total flow rate of 20 sccm (10% propane balanced with Ar) in a quartz tube reactor (0.5 in diameter). About 100 mg catalyst was diluted with 1000 mg 100-mesh SiC to ensure a uniform bed and minimal pressure drop. Quartz wool plugs top and bottom of the catalyst bed were used to fix the bed in the tube. Reactions were performed at ambient pressure. Flow rates of propane (research grade, Airgas), and argon (UHP, Airgas) were controlled using two mass flow controllers (MKS). The outlet stream was analyzed every half hour using an on-line gas chromatograph (SRI) equipped

with a HayeSep-D column and a flame ionization detector (FID) and a thermal conductivity detector (TCD). A thermocouple was introduced directly above the catalyst bed inside the quartz tube for temperature control.

Control Reactions

Tests of an empty reactor, reactor with Al_2O_3 or Al_2O_3 and SiC show little to no conversion and a selectivity of ∼50% towards propylene. Tests of Ga/Al_2O_3 without Ni added showed very low levels of conversion, high initial selectivity, and moderate deactivation over time suggesting that Ni was required to enhance conversion and present new surface chemistry that sustains high selectivity. Tests were also performed over SiO_2 and Ga/SiO_2. Pure SiO_2 showed no reaction. Ga/SiO_2, interestingly, showed moderately high selectivity after a short induction time yet quite low conversion. Ga/SiO_2 also started to deactivate rapidly after ∼11 hours under reaction conditions (Figure S18).

Comparison with Industrial Catalysts

Comparing our results to common commercial catalyst formulations prepared and tested in our lab, the (1:1 Ni:Ga)@Ni_3Ga/Al_2O_3 catalyst exhibited either similar or superior activity and selectivity. Performance comparison of the catalysts Pt+Sn/Al_2O_3 and CrO_x/Al_2O_3 catalysts are presented in Figure S9 and S10. Both the industrial catalyst compositions showed similarly high selectivity towards propylene production at the beginning of the run, yet the CrO_x/Al_2O_3 catalyst suffered from more significant deactivation within 10 hours likely due to surface oxygen loss, coking, and sintering.[6,8–10] The Pt+Sn catalyst was more stable, but deactivated marginally more quickly than the (1:1 Ni:Ga)@Ni_3Ga/Al_2O_3 catalyst. Sintering has been proposed as the source of the observed deactivation of the Pt+Sn catalyst.[5–7] With respect to regeneration, the CrO_x/Al_2O_3 catalyst is commonly run only for a short time and regenerated by simple reoxidation.[6] However, the Pt+Sn catalyst requires aggressive oxidation with molecular Cl_2 to redistribute the Pt and Sn across the oxide surface.[6,11] The

regeneration of the (1:1 Ni:Ga)@Ni_3Ga/Al_2O_3 catalyst is practically similar to that of CrO_x with an added reduction step after initial oxidation. This regeneration is more advantageous than that used for Pt+Sn catalyst due to the use of Cl_2.[6,7]

Investigation on Induction Time as a Function of Surface Ni: Ga Compositions

Induction time and the accompanying unselective conversion of propane tracked inversely as a function of the Ga concentration suggesting that Ni-rich regions of the catalyst were blocked either by Ga or by carbon through coke formation (Figure 3a). This trend was reminiscent of those encountered in approaches aimed at improving selectivity where inert atoms are added to catalysts or surfaces to block overly reactive sites, e.g., Au or Bi.[12,13] Trends in propane conversion also tracked inversely with the Ga loading. High and mostly unselective conversion occurred at the Ni:Ga 3:1 actual loading and decreased systematically until the limit of Ni:Ga of 1:2 where activity towards propane activation was significantly diminished. At the actual loading of Ni:Ga 1:2, similar conversion and activity to the Ga/Al_2O_3 catalyst was observed. Albeit, less deactivation occurred in comparison to the Ga-only catalyst showing the presence of Ni was crucial.

Characterization

TEM and EDS

The characterization of Ni_3Ga/Al_2O_3 and SiO_2 supported Ni+Ga IMC compounds with and without annealing treatment was performed using a variety of techniques. TEM, STEM HAADF, and HR-EDS measurements have been performed on Talos FEI F200X operating at 200 KV at Oak Ridge National Lab (ORNL). TEM and STEM HAADF measurements on annealed Ni_3Ga/SiO_2 were performed on ZEISS LIBRA 120 operating at 120 KV at ORNL.

Holey carbon TEM grids were used. Catalysts were dispersed in methanol and sonicated before being deposited on the TEM grids.

pXRD and HR-pXRD

XRD patterns were measured on a PANalytical X'Pert Pro system using Cu Ka radiation (ORNL) for a minimum of three hours per sample. High resolution synchrotron powder diffraction (HR-XRD) data were collected using the mail-in service at the beamline 11-BM at the Advanced Photon Source (APS), Argonne National Laboratory using an average wavelength of 0.41 . The scan of HR-XRD covered the 2θ range 0.5-50 degree with a step size of 0.001 degree and scan speed of 0.01 degree/s.

High Sensitivity Low Energy Ion Scattering

The High Sensitivity-Low Energy Ion Scattering (HS-LEIS) spectroscopy was utilized to characterize the surface composition of (1:1 Ni:Ga)@Ni_3Ga/Al_2O_3 before and after reaction and Ni_3Ga/SiO_2 with and without annealing treatment. LEIS spectra were collected utilizing an IONTOF Qtac100 spectrometer (Lehigh University). Briefly, the samples were prepared for analysis by compressing powder into LEIS sample holders with filter paper over the powder to prevent contamination from the press. Each sample was then exposed to room temperature H atoms generated from a plasma source for 30 min. Ne+ ions with the energy of 5 keV were utilized to probe the Ni and Ga elements. An ion dose of 5 x 10^{14} cm^{-2} was first used over a wider energy range to provide better signal-to-noise ratio and seek potential contamination from heavier atoms. After that, 1 x 10^{14} cm^{-2} was performed to collect data with less concomitant surface damage during the analysis. In LEIS experiments, the signal in an individual LEIS spectrum, particularly using a Ne+ probe, is almost entirely due to the top exposed atomic layer of the material. The theory is that if a Ne+ probe ion were to penetrate beyond the immediate surface of the sample, it would take an electron from the surrounding material and become neutral. If that projectile subsequently scatters

from a buried atom and reemerges from the sample surface as a neutral Ne, it would not be detectable by the spectrometer.[14,15] If it were to be re-ionized upon leaving the sample, which is unlikely for Ne but more common when using a He+ probe, it would emerge at a kinetic energy lower than that corresponding to an atom at the surface of the target element. For the quantification of surface elemental composition, calibration is needed by measuring either the pure metal or metal oxide,[15–21] or performing depth profiling and utilize the bulk composition as the reference.[22–27] The annealed Ni_3Ga/SiO_2 catalyst was utilized as a well-defined standard since it exhibits pure phase Ni_3Ga bulk crystal structure, relatively uniform particle size (∼6.8 nm), and not suffer from Ga sticking on the surface. Therefore, the ratios of the integrated scattering intensity of Ni to Ga at the end of depth profiles (in the range of ∼2-3 nm) were normalized to the bulk stoichiometry and utilized as reference value to estimate the elemental composition at other layers.

In the current work, the theoretical estimation of surface atomic density of Ni_3Ga is on the order of 10^{15} atoms/cm^2, which coincides with the general assumption of surface atomic density over a wide range of materials in published work.[16,17,26–32] A dose of ion fluence of 1x10^{15} ions cm^{-2} with a sputter beam of 0.5 keV Ar^+ was then estimated to remove ∼1 atomic layer (∼0.3 nm).[17,18,22–27,29,30,33–35] It is also noted that an accurate sputtering rate is difficult to determine since it is affected by many factors such as atomic weight, elemental sputtering yield, material density, actual elemental composition, and crystallographic structure in the outermost surface region. Therefore, we still utilized the estimation that a dose of ion fluence of 1x10^{15} ions cm^{-2} corresponds for a removal of one atomic layer based on literature suggestion.[17,18,22–27,29,30,33–35]

The depth profiling study in this work was performed utilizing a sputter beam of 0.5 keV Ar^+ with a total ion fluence of about 4 x 10^{14} ions cm^{-2} per cycle. Therefore, approximate 0.1 nm atomic layer was removed per cycle. The depth profiling study on the annealed Ni_3Ga/SiO_2 catalyst showed that the surface elemental composition is similar to bulk. The depth profiling study was also performed over (1:1 Ni:Ga)@Ni_3Ga/Al_2O_3 before and after

reaction.

ICP-OES

The elemental analysis was performed using Agilent Technologies 5110 ICP-OES over all supported Ni+Ga catalysts (see Table S1) at the University of Tennessee, Knoxville. The commercial ICP standards of Ni and Ga (100 g/L in 5% nitric acid aqueous solution, Sigma Aldrich) were utilized for calibrations. The synthesized Ni+Ga catalysts were autoclaved at 100°C overnight in the mixture of diluted HF and HNO_3 acids to ensure they were completely dissolved before ICP measurements.

Chemisorption

The amount of active metal sites for the calculation of TOF was determined via chemisorption of H_2 and CO by using Autosorb-iQ/MP-XR. About 0.2 g sample was applied in the chemisorption measurements. The sample was first outgassed at room temperature, heated up to 400°C under a flow of H_2 (80 sccm), and then kept at this temperature for 2 hours. After this treatment, the sample was outgassed under vacuum (10^{-4} Torr) for 2 hours. Then the sample was cooled down to 40°C. After the pretreatment, the chemisorption of H_2 or CO were performed at 40°C. The isotherms were lineal in the range of used pressures (0-640 torr). The amount of chemisorbed H_2/CO was calculated by extrapolation of the isotherm to pressure zero.

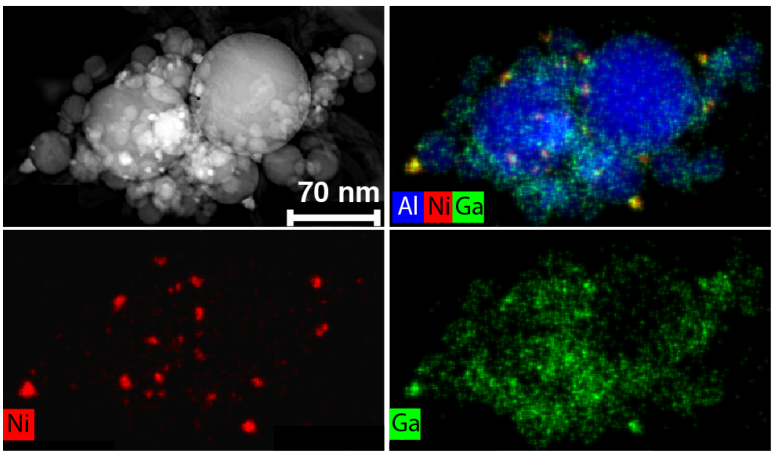

Figure S1: EDX-mapping on (1:1 Ni:Ga)@Ni_3Ga/Al_2O_3 catalyst showing that a portion of Ga atoms interact strongly with the Al_2O_3 support.

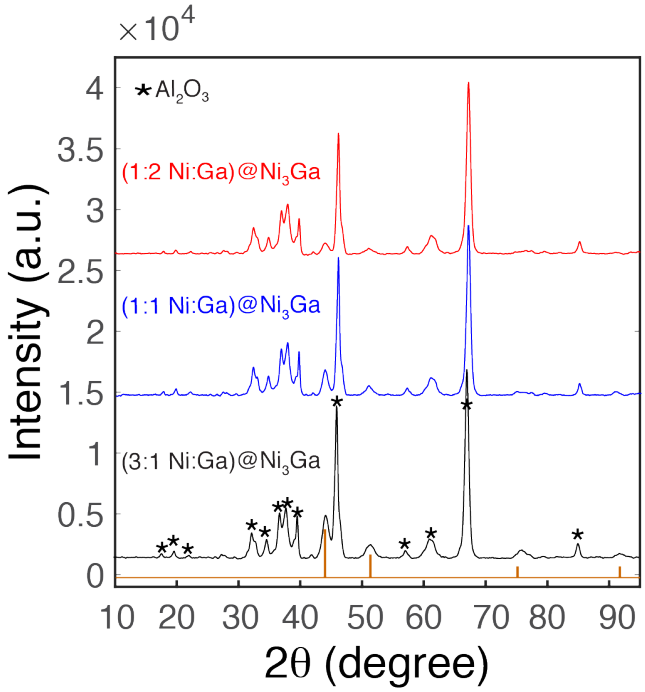

Figure S2: XRD over Al_2O_3 supported Ni+Ga compounds (with actual loading of 3:1, 1:1, and 1:2) showing they all present Ni_3Ga phase in bulk crystal structure regardless of the actual loading change. No unidentified reflections were encountered in the analysis suggesting phase-pure IMC particles.

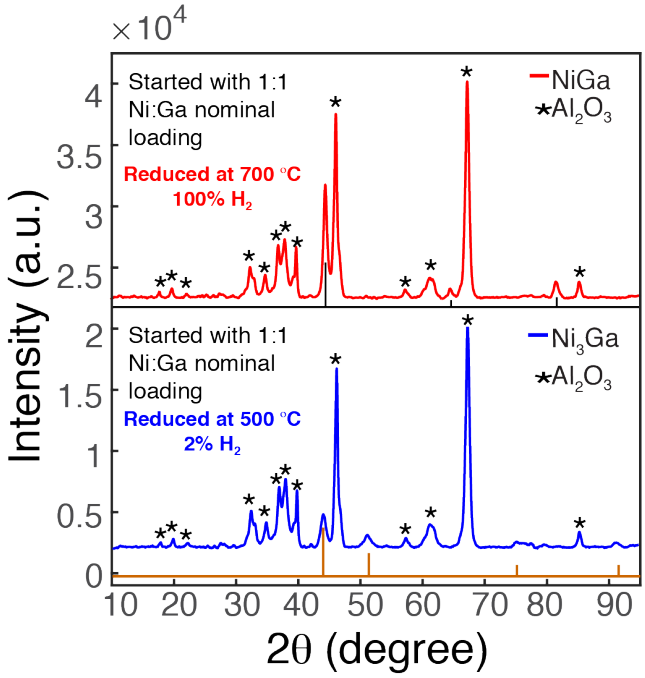

Figure S3: Regular XRD measurements over Al_2O_3 supported Ni+Ga IMCs (with actual loading of 1:1) produced by different pretreatment conditions.

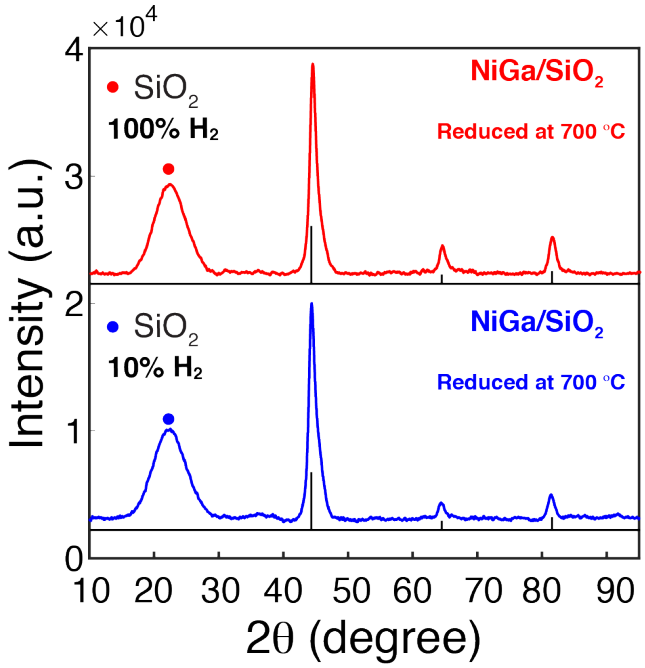

Figure S4: Regular XRD measurements over $NiGa/SiO_2$ with different H_2 concentrations (blue: 10% and red: 100%) in the reduction pretreatment. The results showed that the lower H_2 concentration is sufficient to promote NiGa IMC formation due to the reduced interature between Ga atoms and SiO_2.

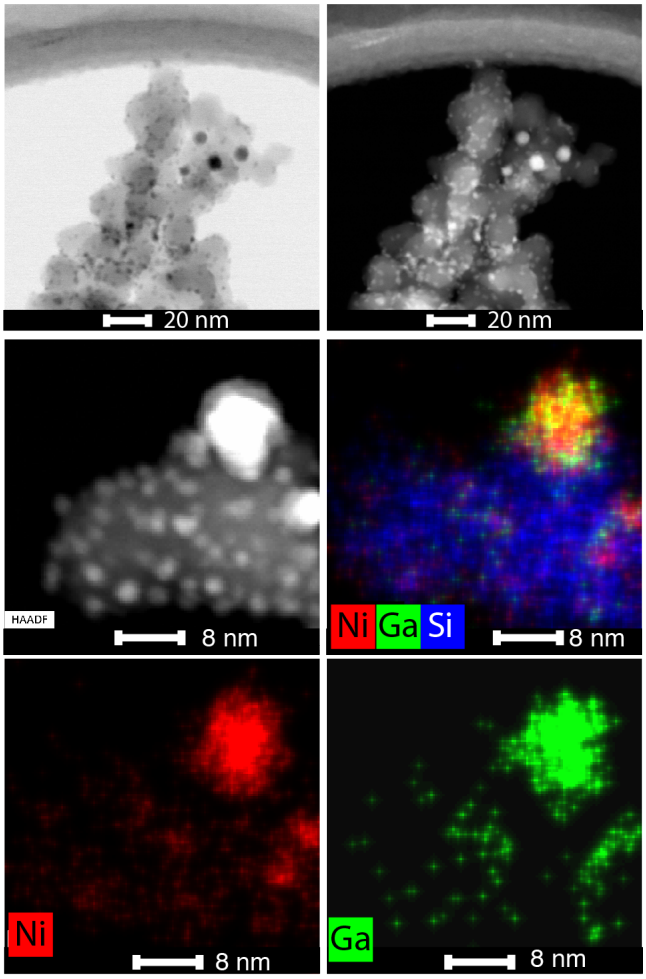

Figure S5 Bright-field and dark-field TEM images and EDX-mapping on fresh Ni_3Ga/SiO_2 catalyst showing that negligible amount of Ga atoms presented on SiO_2 surface.

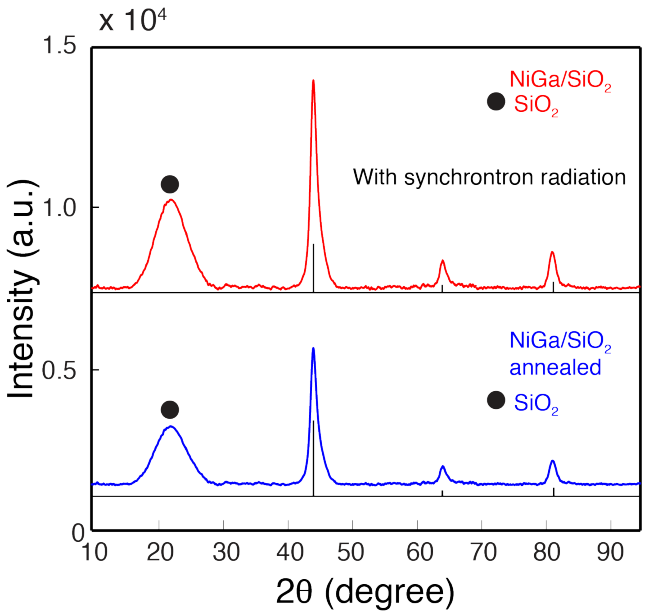

Figure S6 XRD for SiO_2 supported NiGa with (regular XRD) and without annealing pre-treatment (HR-XRD) showing phase-pure NiGa IMC material.

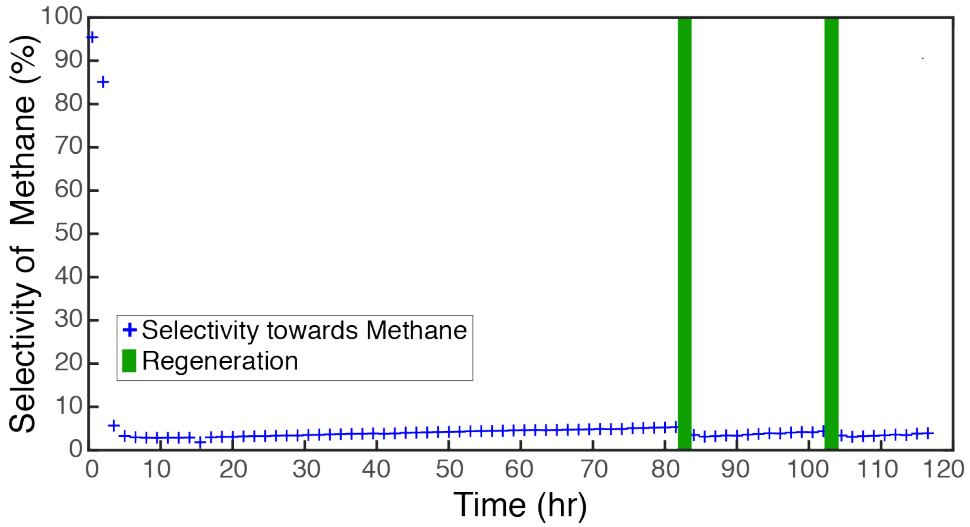

Figure S7: Selectivity towards methane over (1:1 Ni:Ga)@Ni_3Ga/Al_2O_3 in catalytic stability test (Figure 1a) showing a drastic reduction of methane selectivity at the beginning of reaction. This indicated that the overall surface reactivity towards carbon was decreased by the rapid poisoning of highly reactive surface sites at the beginning of the reaction.

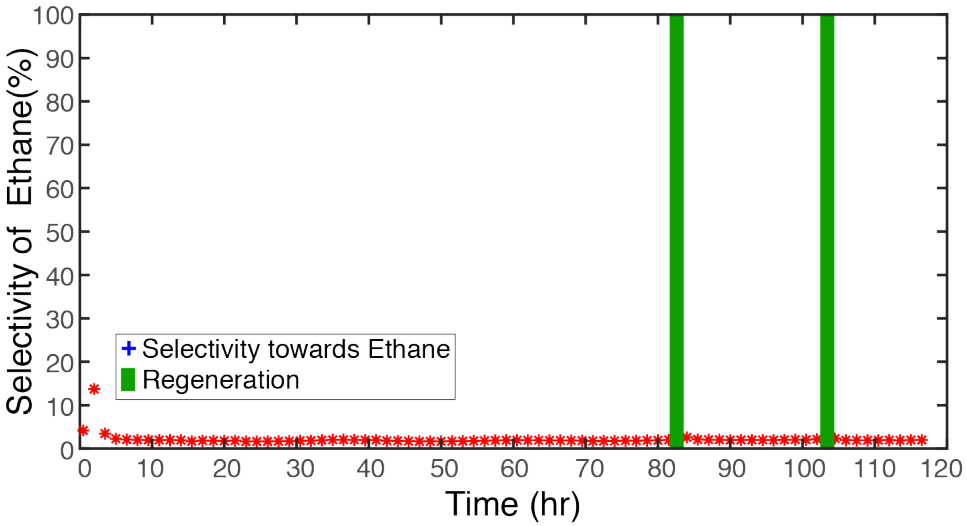

Figure S8: Selectivity towards ethane over (1:1 Ni:Ga)@Ni_3Ga/Al_2O_3 in catalytic stability test (Figure 1a) showing that it is a minor by-product when the catalyst reaches steady state.

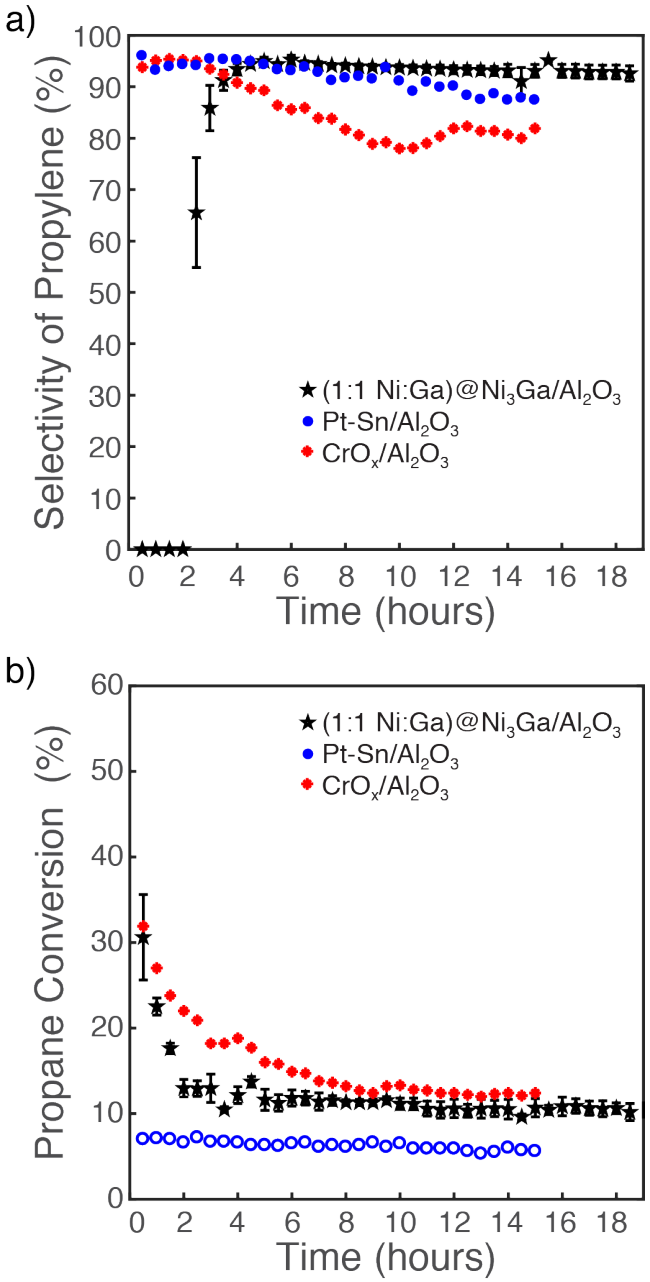

Figure S9: Catalytic performance test of propane dehydrogenation over industrial catalysts (Pt-Sn/Al_2O_3 and CrO_x/Al_2O_3) showing that (1:1 Ni:Ga)@Ni_3Ga/Al_2O_3 catalyst is similar or surpasses the current industrial propane dehydrogenation catalysts in selectivity and activity. The reaction conditions were set as a total flow rate of 20 sccm (10% propane balanced with Ar) at 600°C and under atmospheric pressure.

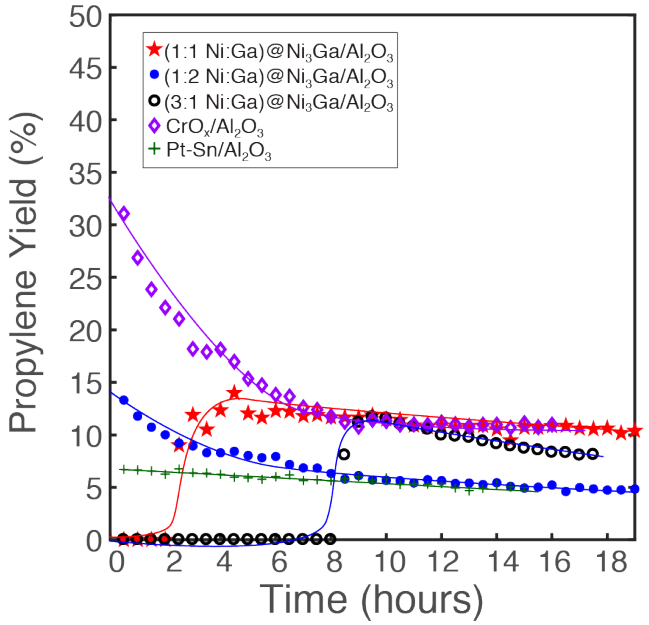

Figure S10: Yield of propylene over (3:1 Ni:Ga)@Ni_3Ga/Al_2O_3, (1:1 Ni:Ga)@Ni_3Ga/Al_2O_3, (1:2 Ni:Ga)@Ni_3Ga/Al_2O_3, and two common industrial catalysts CrO_x/Al_2O_3 and Pt+Sn/Al_2O_3 suggesting an improved catalytic performance over Ni+Ga IMCs.

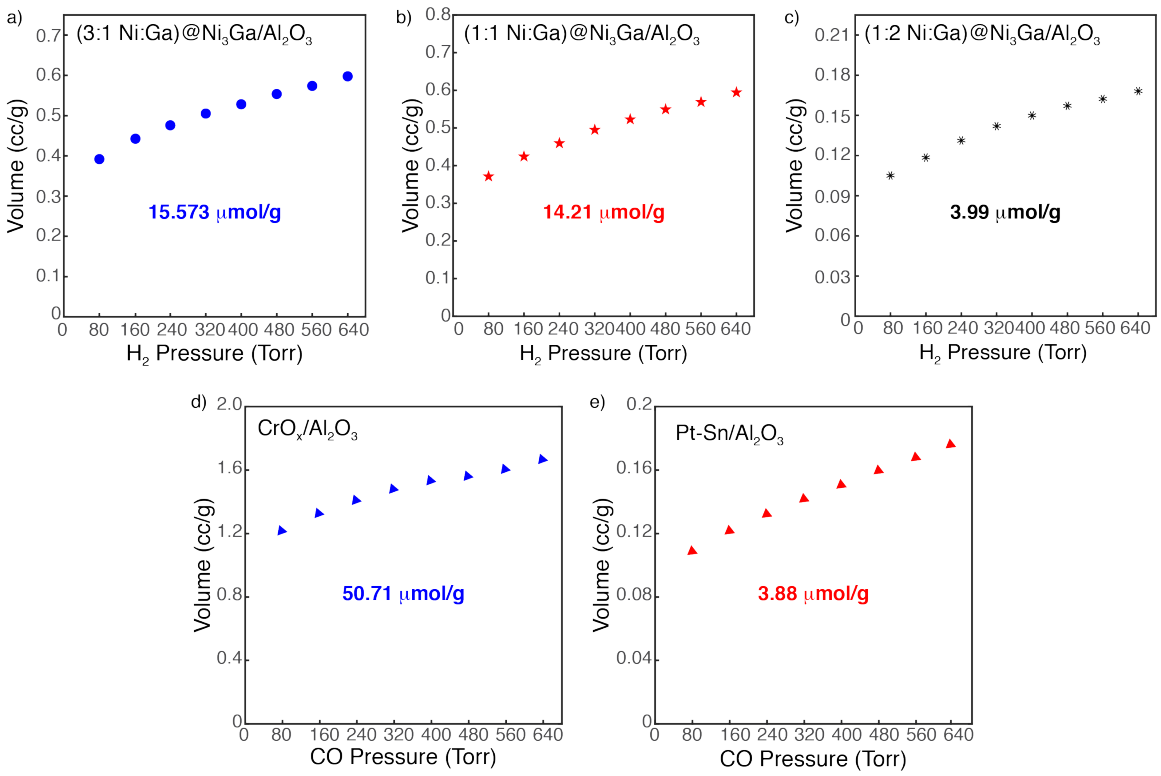

Figure S11: The isotherm plots for H_2/CO chemisorptions utilized to estimate the amount of reaction sites on the surfaces of Al_2O_3 supported Ni+Ga IMC catalysts and the in-house synthesized commercial catalysts, Al_2O_3 supported CrO_x and Pt-Sn. The amount of chemisorbed H_2/CO was calculated by extrapolation of the isotherm to pressure zero.

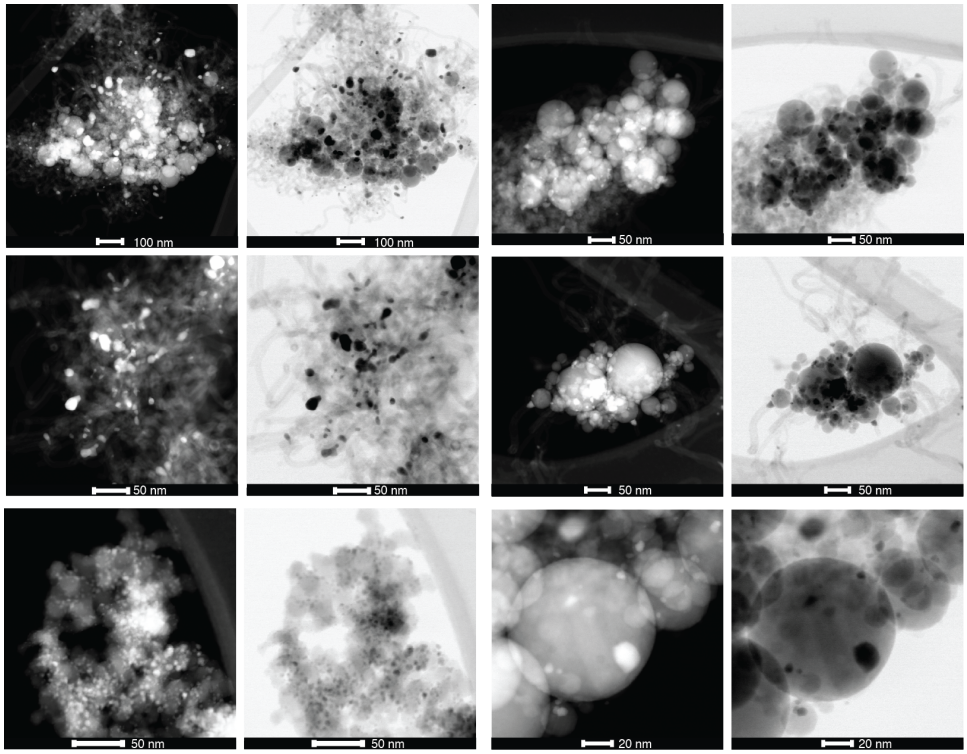

Figure S12: Dark-field and bright-field TEM studies on use (1:1 Ni:Ga)@Ni_3Ga/Al_2O_3 showing that coke formation occurred selectively at small and potentially Ni-rich particles and was of nanotube type. No overlayers of coke on IMC particles were encountered.

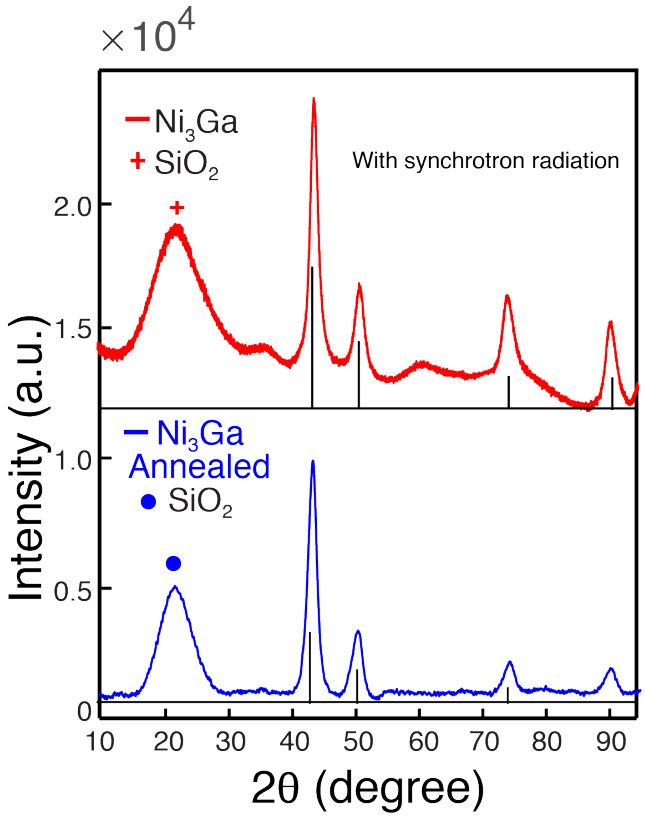

Figure S13: XRD for SiO_2 supported Ni_3Ga (3:1 Ni:Ga actual loading) with (regular XRD, blue) and without annealing pretreatment (HR-XRD, red) showing that the bulk crystal structure of Ni_3Ga is not affected by annealing treatment.

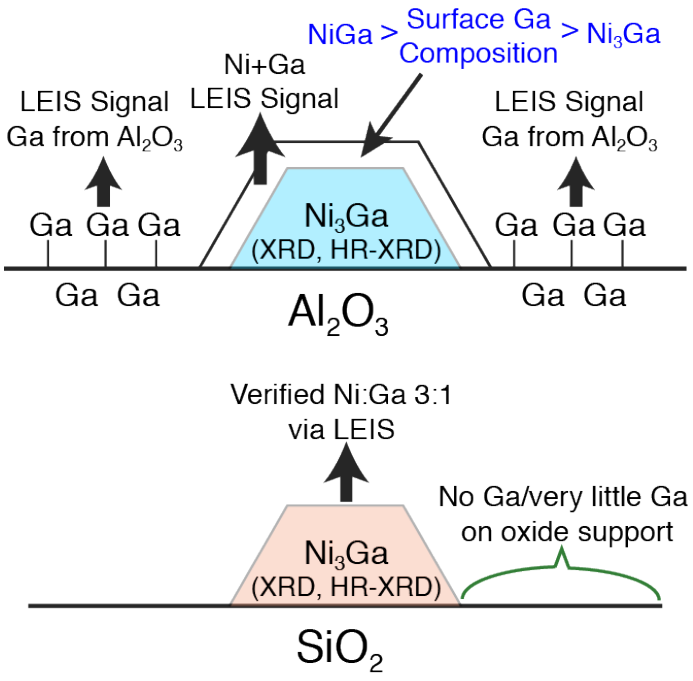

Figure S14: Cartoon for describing the location of Ni and Ga detected by HS-LEIS. The information about the surface composition of Ni_3Ga particle on Al_2O_3 support was convoluted by the Ga atoms that stuck on Al_2O_3 whereas the surface composition can be analyzed more exactly over SiO_2 supported Ni+Ga IMCs.

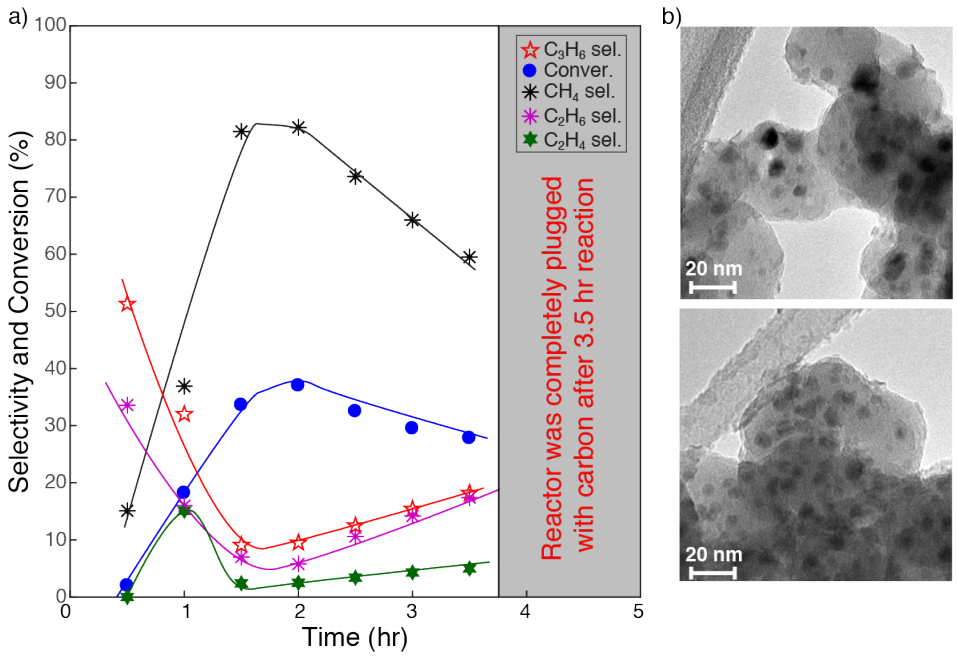

Figure S15: a) Product distributions and propane conversion of propane dehydrogenation reaction over annealed Ni_3Ga/SiO_2 (12 hrs annealing at 700°C under Ar after reduction); b) TEM images showed an average particle size of 6-7 nm indicating only slight particle growth after annealing pretreatment. Results demonstrated that the surface reactivity of Ni_3Ga/SiO_2 after annealing was still too aggressive towards C–C/C=C activation in comparison to (1:1 Ni:Ga)@Ni_3Ga/Al_2O_3 catalyst.

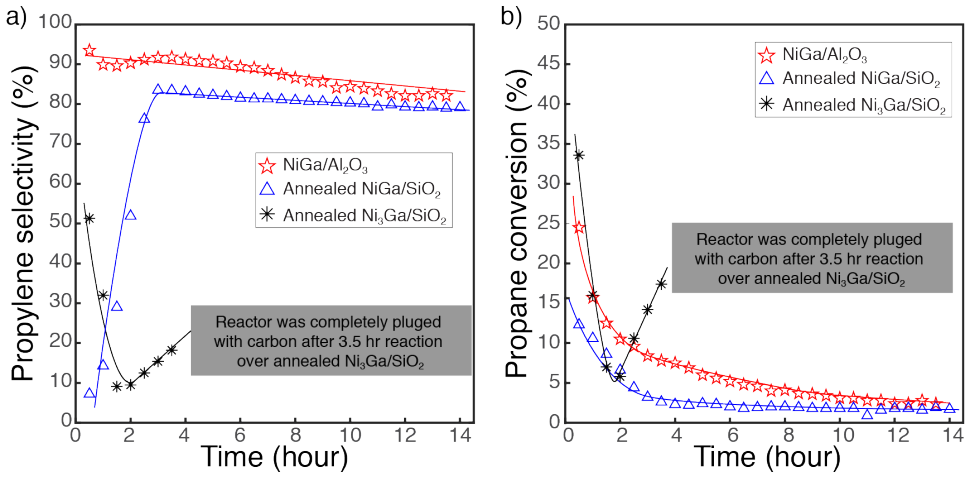

Figure S16: Catalytic performance over well-defined annealed SiO_2 supported NiGa and Ni_3Ga as well as Al_2O_3 supported NiGa catalysts to partially understand the surface composition of (1:1 Ni:Ga)@Ni_3Ga/Al_2O_3 that corresponds for its high performance.

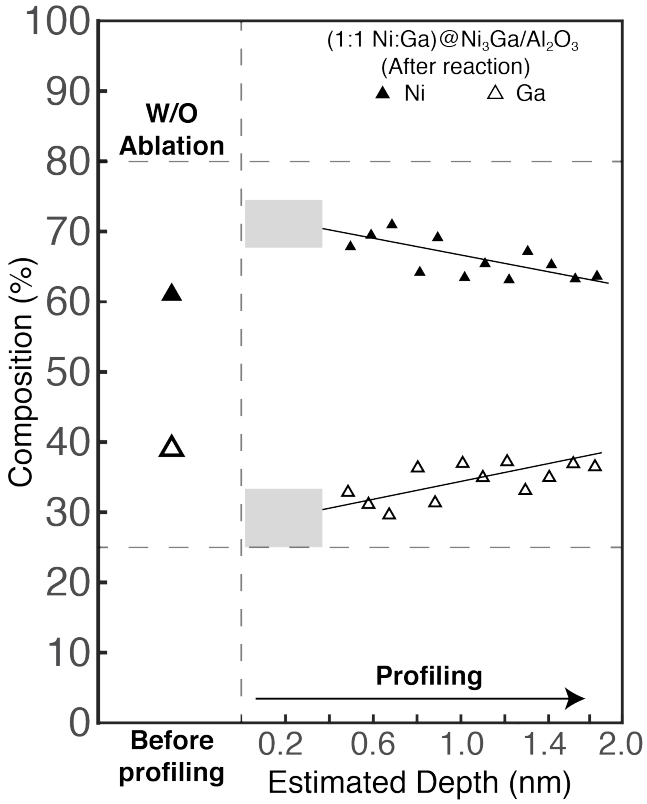

Figure S17: HS-LEIS depth profiling analysis over (1:1 Ni:Ga)@Ni_3Ga/Al_2O_3 catalyst after reaction. It showed an increase of surface Ni composition for the catalyst after reaction. The true surface composition analysis was convoluted by the Ga atoms trapped by oxide support.

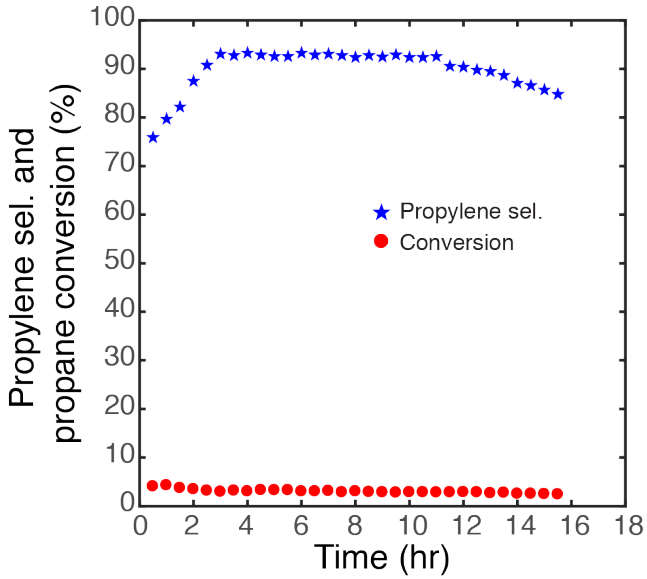

Figure S18: Performance test of propane dehydrogenation over SiO_2 supported Ga showing low conversion of propane and less stability towards propylene selectivity.

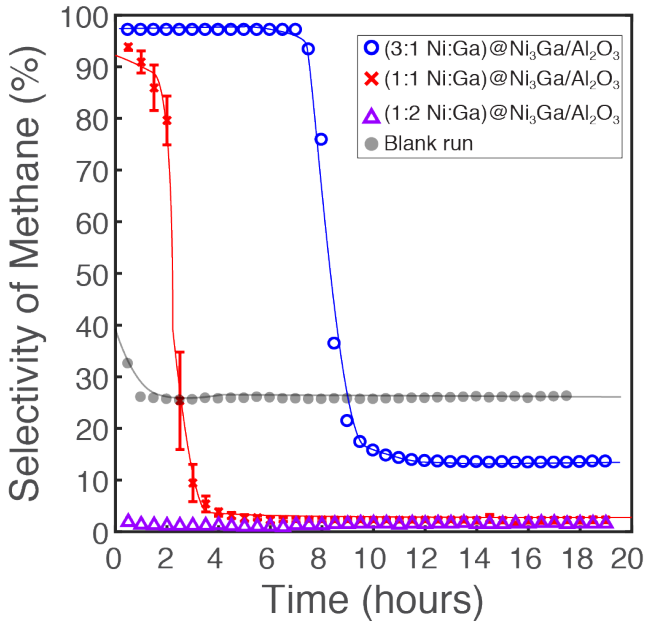

Figure S19: Selectivity towards methane in propane dehydrogenation reaction over Al_2O_3 supported Ni+Ga catalysts with different loadings. The results showed a systematic decrease in surface reactivity towards C–C/C=C bond as more Ga atoms was introduced.

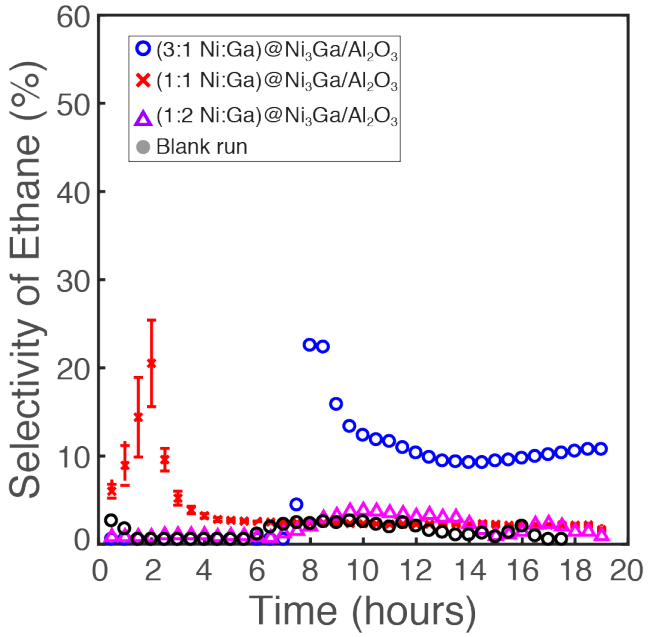

Figure S20: Selectivity towards ethane in propane dehydrogenation reaction over Al_2O_3 supported Ni+Ga catalysts with different loadings. Results indicated that Ni+Ga IMCs with the actual loadings of 3:1 and 1:1 have highly reactive surface sites that drive C-C/C=C bond cleavage and their contribution diminished likely due to site-specific poisoning.

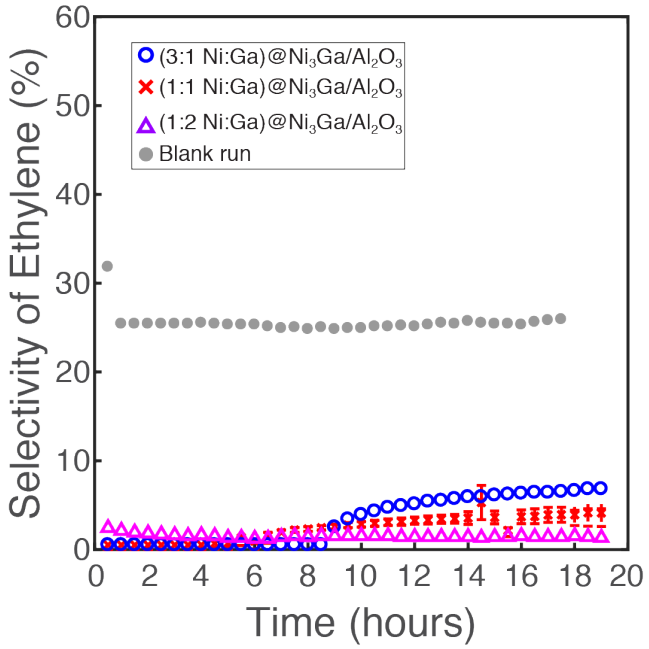

Figure S21: Selectivity towards ethylene in propane dehydrogenation reaction over Al_2O_3 supported Ni+Ga catalysts with different loadings. The results showed a decrease in ethylene selectivity as more Ga atoms were introduced. This aspect indicated a systematic manipulation on surface carbon affinity as a function of Ga composition on surface of Ni_3Ga nanoparticle.

Table S1: ICP-OES quantification of the composition of the supported Ni+Ga catalysts. The number in the parenthesis is the actual loading.

Catalyst	Ni content, mol%	Ga content, mol%
Ni_3Ga/Al_2O_3 (3:1)	75.5 (75)	24.5 (25)
Ni_3Ga/Al_2O_3 (1:1)	49.2 (50)	50.8 (50)
Ni_3Ga/Al_2O_3 (1:2)	33.7 (33.3)	66.3 (66.7)
Ni_3Ga/SiO_2 (3:1)	75.3 (75)	24.7 (25)
$NiGa/SiO_2$ (1:1)	50.9 (50)	40.1 (50)

Table S2: Catalytic production rate and TOF of propylene. The production rate and TOF were reported at the beginning of the steady state over Ni_3Ga/Al_2O_3 (3:1) and Ni_3Ga/Al_2O_3 (1:1), Pt+Sn/Al_2O_3, and CrO_x/Al_2O_3. For Ni_3Ga/Al_2O_3 (1:2) that was not able to reach their steady state, the production rate and TOF of propylene at the beginning and the end (parenthesis) of reaction were reported. The amount of metal reaction sites were determined by H_2 chemisorption for Ni+Ga catalysts and by CO chemisorption for Pt-Sn and CrO_x catalysts. A summary of published supported Pt+Sn and CrO_x was selected from a review[6] and re-tabulated for comparison.

Catalyst	Reaction Temp. (°C)	WHSV (h^{-1})	Feed Composition	TOF (s^{-1})	Ref.
Ni_3Ga/Al_2O_3 (3:1)	600	2.4	C_3H_8 = 10, Ar = 90	4.3 x 10^{-2}	–
Ni_3Ga/Al_2O_3 (1:1)	600	2.4	C_3H_8 = 10, Ar = 90	4.7 x 10^{-2}	–
Ni_3Ga/Al_2O_3 (1:2)	600	2.4	C_3H_8 = 10, Ar = 90	1.1 x 10^{-1} (2.8 x 10^{-2})	–
Pt+Sn/Al_2O_3	600	2.4	C_3H_8 = 10, Ar = 90	4.5 x 10^{-2}	–
CrO_x/Al_2O_3	600	2.4	C_3H_8 = 10, Ar = 90	1.3 x 10^{-3}	–
Pt+Sn-Na/Al-SBA15	590	3.0	C_3H_8 = 75, H_2 = 25	1.4 x 10^{-1}	[36]
Pt+Sn/Al_2O_3	519	3.5	C_3H_8 = 30, N_2 = 70	1.8 x 10^{-1}	[37]
Pt+Sn/$MgAl_2O_3$	550	36.6	C_3H_8 = 50, H_2 = 50	5.0 x 10^{-1}	[38]
CrO_x-Na/Al_2O_3	550	0.1	C_3H_8 = 10, N_2 = 90	7.4 x 10^{-6}	[39]
CrO_x/ZrO_2	550	0.3	C_3H_8 = 2.5, N_2 = 97.5	2.9 x 10^{-5}	[40]
CrO_x/Al_2O_3	580	N/A	C_3H_8 = 10, N_2 = 90	4.7x10^{-3}	[10]

References

(1) He, Y.; Laursen, S. Trends in the Surface and Catalytic Chemistry of Transition-Metal Ceramics in the Deoxygenation of a Woody Biomass Pyrolysis Model Compound. *ACS Catal.* **2017**, *7*, 3169–3180.

(2) He, Y.; Laursen, S. The surface and catalytic chemistry of the first row transition metal phosphides in deoxygenation. *Catalysis Science & Technology* **2018**, *8*, 5302–5314.

(3) Song, Y. Control of Surface Reactivity of Ni+B Group Intermetallic Compounds towards Unsaturated C-C bonds and Hydrogen in Semi-hydrogenation of Acetylene. *J. Catal.* **2018**, *Under review*.

(4) Poudyal, S.; Laursen, S. Insights into Elevated-Temperature Photocatalytic Reduction of CO2 by H2O. *The Journal of Physical Chemistry C* **2018**, *122*, 8045–8057.

(5) Pham, H. N.; Sattler, J. J. H. B.; Weckhuysen, B. M.; Datye, A. K. Role of Sn in

the Regeneration of Pt/γ-Al_2O_3 Light Alkane Dehydrogenation Catalysts. *ACS Catal.* **2016**, *6*, 2257–2264.

(6) Sattler, J. J. H. B.; Ruiz-Martinez, J.; Santillan-Jimenez, E.; Weckhuysen, B. M. Catalytic Dehydrogenation of Light Alkanes on Metals and Metal Oxides. *Chew. Rev.* **2014**, *114*, 10613–10653.

(7) Iglesias-Juez, A.; Beale, A. M.; Maaijen, K.; Weng, T. C.; Glatzel, P.; Weckhuysen, B. M. A Combined in situ Time-resolved UV–Vis, Raman and High-energy Resolution X-ray Absorption Spectroscopy Study on the Deactivation Behavior of Pt and PtSn Propane Dehydrogenation Catalysts under Industrial Reaction Conditions. *J. Catal.* **2010**, *276*, 268–279.

(8) Airaksinen, S. M. K.; Harlin, M. E.; Krause, A. O. I. Kinetic Modeling of Dehydrogenation of Isobutane on Chromia/Alumina Catalyst. *Ind. Eng. Chem. Res.* **2002**, *41*, 5619–5626.

(9) Hakuli, A.; Harlin, M.; Backman, L.; Krause, A. Dehydrogenation of i-Butane on CrO_x/SiO_2 Catalysts. *J. Catal.* **1999**, *184*, 349–356.

(10) Puurunen, R. Spectroscopic Study on the Irreversible Deactivation of Chromia/Alumina Dehydrogenation Catalysts. *J. Catal.* **2002**, *210*, 418–430.

(11) Heyse, J. V.; Johnson, P. G.; Mulaskey, B. F. Dehydrogenation Processes, Equipment and Catalyst Loads Therefor. *Patent US5723707A* **1993**,

(12) Yan, Z.; Yao, Y.; Goodman, D. W. Dehydrogenation of Propane to Propylene over Supported Model Ni–Au Catalysts. *Catal. Lett.* **2012**, *142*, 714–717.

(13) Molenbroek, A. M.; Nørskov, J. K.; Clausen, B. S. Structure and Reactivity of Ni-Au Nanoparticle Catalysts. *J. Phys. Chem. B* **2001**, *105*, 5450–5458.

(14) Cushman, C. V.; Brüner, P.; Zakel, J.; Major, G. H.; Lunt, B. M.; Smith, N. J.; Grehl, T.; Linford, M. R. Low energy ion scattering (LEIS). A practical introduction to its theory, instrumentation, and applications. *Anal. Methods* **2016**, *8*, 3419–3439.

(15) Brongersma, H. H. Low-Energy Ion Scattering. *Characterization of Materials* **2012**,

(16) ter Veen, H.; Kim, T.; Wachs, I.; Brongersma, H. Applications of High Sensitivity-Low Energy Ion Scattering (HS-LEIS) in heterogeneous catalysis. *Catalysis Today* **2009**, *140*, 197–201.

(17) Phivilay, S. P.; Roberts, C. A.; Puretzky, A. A.; Domen, K.; Wachs, I. E. Fundamental Bulk/Surface Structure–Photoactivity Relationships of Supported (Rh2–yCryO3)/GaN Photocatalysts. *The Journal of Physical Chemistry Letters* **2013**, *4*, 3719–3724.

(18) Phivilay, S. P.; Roberts, C. A.; Gamalski, A. D.; Stach, E. A.; Zhang, S.; Nguyen, L.; Tang, Y.; Xiong, A.; Puretzky, A. A.; Tao, F. F.; et al., Anatomy of a Visible Light Activated Photocatalyst for Water Splitting. *ACS Catalysis* **2018**, *8*, 6650–6658.

(19) Li, Y.; Hu, J.; Ma, D.; Zheng, Y.; Chen, M.; Wan, H. Disclosure of the Surface Composition of TiO2-Supported Gold–Palladium Bimetallic Catalysts by High-Sensitivity Low-Energy Ion Scattering Spectroscopy. *ACS Catalysis* **2018**, *8*, 1790–1795.

(20) Hemmingson, S. L.; Feeley, G. M.; Miyake, N. J.; Campbell, C. T. Energetics of 2D and 3D Gold Nanoparticles on MgO(100): Influence of Particle Size and Defects on Gold Adsorption and Adhesion Energies. *ACS Catalysis* **2017**, *7*, 2151–2163.

(21) Zheng, J.; Qu, J.; Lin, H.; Zhang, Q.; Yuan, X.; Yang, Y.; Yuan, Y. Surface Composition Control of the Binary Au–Ag Catalyst for Enhanced Oxidant-Free Dehydrogenation. *ACS Catalysis* **2016**, *6*, 6662–6669.

(22) Foo, G. S.; Polo-Garzon, F.; Fung, V.; Jiang, D.-e.; Overbury, S. H.; Wu, Z. Acid–Base

Reactivity of Perovskite Catalysts Probed via Conversion of 2-Propanol over Titanates and Zirconates. *ACS Catalysis* **2017**, *7*, 4423–4434.

(23) Polo-Garzon, F.; Yang, S.-Z.; Fung, V.; Foo, G. S.; Bickel, E. E.; Chisholm, M. F.; Jiang, D.-e.; Wu, Z. Controlling Reaction Selectivity through the Surface Termination of Perovskite Catalysts. *Angewandte Chemie International Edition* **2017**, *56*, 9820–9824.

(24) Foo, G. S.; Hood, Z. D.; Wu, Z. Shape Effect Undermined by Surface Reconstruction: Ethanol Dehydrogenation over Shape-Controlled SrTiO3 Nanocrystals. *ACS Catalysis* **2017**, *8*, 555–565.

(25) Rupp, G. M.; Téllez, H.; Druce, J.; Limbeck, A.; Ishihara, T.; Kilner, J.; Fleig, J. Surface chemistry of La0.6Sr0.4CoO3âĹŠÎť thin films and its impact on the oxygen surface exchange resistance. *Journal of Materials Chemistry A* **2015**, *3*, 22759–22769.

(26) Li, C.; Pramana, S. S.; Ni, N.; Kilner, J.; Skinner, S. J. Surface Chemistry of La0.99Sr0.01NbO4-d and Its Implication for Proton Conduction. *ACS Appl. Mater. Interfaces* **2017**, *9*, 29633–29642.

(27) Druce, J.; Téllez, H.; Burriel, M.; Sharp, M. D.; Fawcett, L. J.; Cook, S. N.; McPhail, D. S.; Ishihara, T.; Brongersma, H. H.; Kilner, J. A. Surface termination and subsurface restructuring of perovskite-based solid oxide electrode materials. *Energy Environ. Sci.* **2014**, *7*, 3593–3599.

(28) Stadlmayr, W.; Huber, V.; Penner, S.; Klötzer, B.; Memmel, N. Alloying and Structure of Ultrathin Gallium Films on the (111) and (110) Surfaces of Palladium. *The Journal of Physical Chemistry C* **2013**, *117*, 19558–19567.

(29) Phivilay, S. P.; Puretzky, A. A.; Domen, K.; Wachs, I. E. Nature of Catalytic Active Sites Present on the Surface of Advanced Bulk Tantalum Mixed Oxide Photocatalysts. *ACS Catal.* **2013**, *3*, 2920–2929.

(30) Dittmer, A.; Menze, J.; Mei, B.; Strunk, J.; Luftman, H. S.; Gutkowski, R.; Wachs, I. E.; Schuhmann, W.; Muhler, M. Surface Structure and Photocatalytic Properties of Bi2WO6 Nanoplatelets Modified by Molybdena Islands from Chemical Vapor Deposition. *The Journal of Physical Chemistry C* **2016**, *120*, 18191–18200.

(31) Mayr, L.; Lorenz, H.; Armbrüster, M.; Villaseca, S. A.; Luo, Y.; Cardoso, R.; Burkhardt, U.; Zemlyanov, D.; Haevecker, M.; Blume, R.; et al., The catalytic properties of thin film Pd-rich GaPd2 in methanol steam reforming. *Journal of Catalysis* **2014**, *309*, 231–240.

(32) Hermann, P.; Guigner, J.; Tardy, B.; Jugnet, Y.; Simon, D.; Bertolini, J.-C. The Pd/Ni(110) Bimetallic System: Surface Characterisation by LEED, AES, XPS, and LEIS Techniques; New Insight on Catalytic Properties. *Journal of Catalysis* **1996**, *163*, 169–175.

(33) Zhu, M.; YalçÄśn, Ö.; Wachs, I. E. Revealing structure-activity relationships in chromium free high temperature shift catalysts promoted by earth abundant elements. *Appl. Catal. B* **2018**, *232*, 205–212.

(34) Gao, Y.; Haeri, F.; He, F.; Li, F. Alkali Metal-Promoted LaxSr2–xFeO4âĹŠÎť Redox Catalysts for Chemical Looping Oxidative Dehydrogenation of Ethane. *ACS Catalysis* **2018**, *8*, 1757–1766.

(35) Zhu, M.; Rocha, T. C. R.; Lunkenbein, T.; Knop-Gericke, A.; Schlögl, R.; Wachs, I. E. Promotion Mechanisms of Iron Oxide-Based High Temperature Water–Gas Shift Catalysts by Chromium and Copper. *ACS Catalysis* **2016**, *6*, 4455–4464.

(36) Duan, Y.; Zhou, Y.; Zhang, Y.; Sheng, X.; Xue, M. Effect of Sodium Addition to PtSn/AlSBA-15 on the Catalytic Properties in Propane Dehydrogenation. *Catalysis Letters* **2010**, *141*, 120–127.

(37) Bariås, O. A.; Holmen, A.; Blekkan, E. A. Propane Dehydrogenation over Supported Pt and Pt–Sn Catalysts: Catalyst Preparation, Characterization, and Activity Measurements. *Journal of Catalysis* **1996**, *158*, 1–12.

(38) Salmones, J.; Wang, J.-A.; Galicia, J. A.; Aguilar-Rios, G. H2 reduction behaviors and catalytic performance of bimetallic tin-modified platinum catalysts for propane dehydrogenation. *Journal of Molecular Catalysis A: Chemical* **2002**, *184*, 203–213.

(39) Sattler, J. J. H. B.; González-Jiménez, I. D.; Mens, A. M.; Arias, M.; Visser, T.; Weckhuysen, B. M. Operando UV-Vis spectroscopy of a catalytic solid in a pilot-scale reactor: deactivation of a CrOx/Al2O3 propane dehydrogenation catalyst. *Chemical Communications* **2013**, *49*, 1518.

(40) Zhang, X.; Yue, Y.; Gao, Z. Chromium Oxide Supported on Mesoporous SBA-15 as Propane Dehydrogenation and Oxidative Dehydrogenation Catalysts. *Catalysis Letters* **2002**, *83*, 19–25.